Kusumah, Ferdi Perdana; Kyyrä, Jorma

Successive injections modulation of a direct three-phase to single-phase AC/AC converter for a contactless electric vehicle charger

Published in:
The Journal of Engineering

DOI:
10.1049/joe.2018.8076

Published: 01/01/2019

Document Version
Publisher's PDF, also known as Version of record

The Journal of Engineering

The 9th International Conference on Power Electronics, Machines and Drives (PEMD 2018)

IET Journals
The Institution of Engineering and Technology

Successive injections modulation of a direct three-phase to single-phase AC/AC converter for a contactless electric vehicle charger

eISSN 2051-3305
Received on 22nd June 2018
Accepted on 2nd August 2018
E-First on 26th April 2019
doi: 10.1049/joe.2018.8076
www.ietdl.org

Ferdi Perdana Kusumah[1] ✉, *Jorma Kyyrä*[1]

[1]*Department of Electrical Engineering and Automation, School of Electrical Engineering AALTO UNIVERSITY, P.O. Box 13000, FI-00076 Aalto, Finland*

✉ *E-mail: ferdi.kusumah@aalto.fi*

Abstract: This paper proposes a successive injection modulation (SIM) method for a direct three-phase to single-phase AC/AC converter of a contactless electric vehicle (EV) charger. The converter has a fewer bi-directional switches than a matrix converter without a neutral line connection. It operates using injection and free-wheeling oscillation commutations based on a zero-current switching mechanism. Analytical calculations were derived using a steady-state analysis. Simulation results were obtained to validate the calculations. The proposed modulation increases output power three times compared to a non-successive one with the same circuit setup.

1 Introduction

A direct three-phase to single-phase AC/AC converter for an inductive contactless power transfer (ICPT) system has been published in [1, 2]. It has a fewer number of bi-directional switches than a matrix converter without a neutral line connection and connected to a resonant circuit. It uses a phase shift modulation strategy, which is based on a hard-switching principle and uses a constant switching frequency that leads to losses and reduced transfer efficiency when system parameter values are varied [2, 3]. Other modulation strategy of the same topology were proposed in [4–6]. It is based on injection and free-wheeling oscillation commutations, which were initially presented in [7–9]. The switching transition is performed at a zero-crossing of the primary resonant circuit current to reduce switching losses. In this case, the switching frequency will always be the same as the resonant frequency, so a maximum transfer efficiency is always maintained. However, the modulation only uses one input phase most of the time instead of the full-potential of line-to-line three-phase input, thus the average output power is limited [4].

A successive injection modulation (SIM) strategy is proposed here. It permits positive and negative injections usage successively, so the line-to-line three-phase input is utilised. The modulation produces a bigger output power at a maximum output capacity operation compared to the modulation in [4] for the same circuit setup. The final prototype of the ICPT system will be used to charge an electric vehicle (EV).

This paper is organised as follows. In Section 2, circuit topology, commutations, and previous modulation scheme are explained. Section 3 describes a basic principle of SIM and how it is applied. Steady-state analysis is also given in the section. Fourth section analyses some simulation results under certain conditions. Finally, conclusions of the paper are drawn.

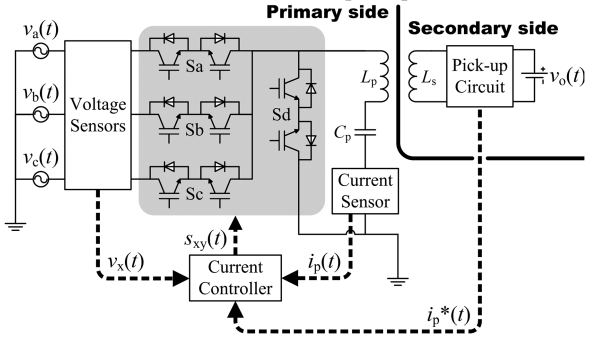

Fig. 1 *ICPT system schematic. Grey area highlights bi-directional switches connections of the AC/AC converter*

2 System characteristics

2.1 Converter topology and commutations

Schematic drawing of the ICPT system with an emphasis to its primary-side topology is illustrated in Fig. 1. The primary circuit side AC/AC converter contains four bi-directional switches and a resonant circuit L_p and C_p. Switch pairs of *S*a, *S*b and *S*c are connected in series with the three-phase input and connected to the ground through the resonant circuit. The *S*d switch pair is connected in parallel with the resonant circuit. Primary and secondary inductors L_p and L_s are magnetically coupled. The pick-up circuit is connected to an EV's battery $v_o(t)$.

An on-off current controller is used in this case to control the primary current amplitude i_p(t) through $s_{xy}(t)$ signal that leads to a controlled output power. It receives $v_x(t)$ and $i_p(t)$ information from voltage and current sensors, respectively, as well as $i_p^*(t)$ set point from the secondary pick-up circuit. Subscript 'x' indicates each input phase, while 'y' is a current direction. Positive direction is defined as a flow that goes towards the resonant circuit, while negative direction is the other way around.

Four main commutations that are used by the converter are shown in Fig. 2. Positive and negative injections are illustrated in Figs. 2*a* and *b,* respectively. They belong to situations where the primary resonant current flows either from one-phase to the resonant circuit or vice versa. The same principle applies to the other two phases. Figs. 2*c* and *d* are free-wheeling oscillation cases, where the current only oscillates in the resonant circuit.

2.2 Non-successive injection modulation

Non-SIM (NIM) refers to the modulation described in [4]. The process is illustrated in Fig. 3 for a case of a controlled output, due to the sparseness of injection voltage $v_{in}(t)$. It drives the primary resonant current during:

$$\mathrm{Max}(v) = \mathrm{Max}(|v_a(t)|, |v_b(t)|, |v_c(t)|)\,. \tag{1}$$

The injection is followed by the free-wheeling oscillation most of the time. Transition between the commutations is performed at a zero-crossing of a primary resonant current $i_p(t)$. This can be seen

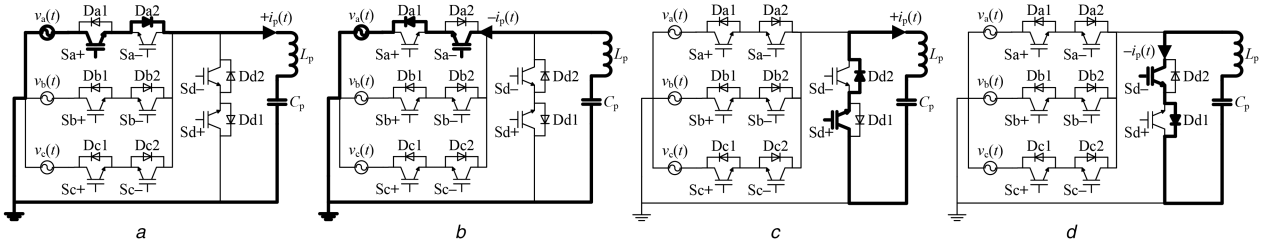

Fig. 2 *Simplified schematic of a primary side ICPT system. Injection commutations are marked by* ***(a)*** and ***(b)***, while ***(c)*** and ***(d)*** Indicate free-wheeling oscillations

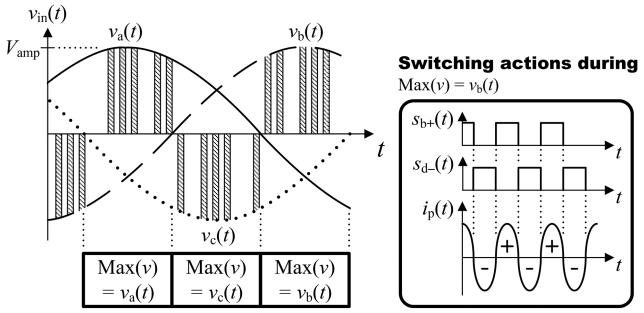

Fig. 3 *Non-successive injection modulation illustration. Each phase voltage amplitude is V_{amp}. The right waveforms are a case when Max(v) equals $v_b(t)$. The switching signals correspond to the IGBTs depicted in Fig. 2*

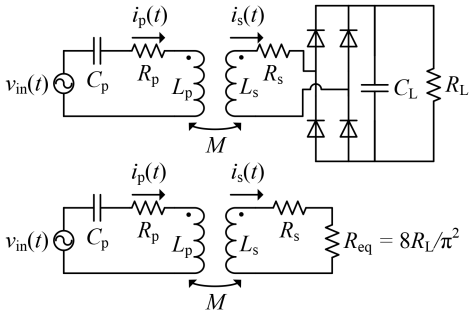

Fig. 4 *Equivalent circuit model of ICPT system with a secondary side rectifier connected to a capacitor C_L and a purely resistive load R_L*

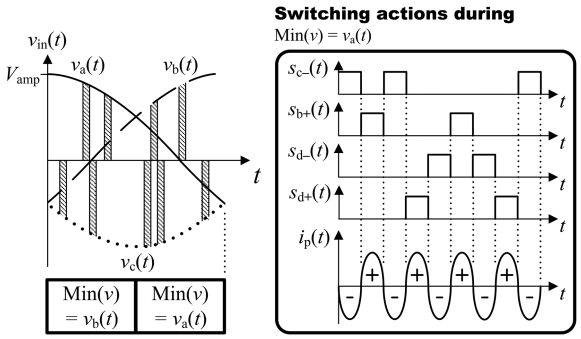

Fig. 5 *Successive injection modulation illustration. Each phase voltage amplitude is V_{amp}. The right waveforms are a case during Min(v) equals $v_a(t)$. The switching signals correspond to the IGBTs depicted in Fig. 2*

on the highlighted switching actions part of the figure. The polarity of injection voltage is always the same as the polarity of the resonant current [4].

Some steady-state variables of NIM can be obtained through a model provided in Fig. 4. They are derived using some assumptions, which are, all electric components are ideal, the load is purely resistive, and the converter is at a maximum output capacity condition. Variables R_p and R_s are primary and secondary coil resistances correspondingly. Primary and secondary currents are indicated by $i_p(t)$ and $i_s(t)$. Mutual inductance between two circuit sides is marked by M. The injection voltage is approximated by a fundamental harmonic analysis given in [4]. The top schematic of Fig. 4 is simplified further to the bottom one through an approach explained in [10].

The primary resonant current $\boldsymbol{i_p}$ and output power P_{out} can be calculated with following equations

$$\boldsymbol{i}_p = \boldsymbol{V_s}/\left[R_p + \frac{\omega_0^2 M(R_s + R_{eq})}{(R_s + R_{eq})^2 + \omega_0^2 L_s^2}\right], \tag{2}$$

$$P_{out} = |\boldsymbol{i}_s|^2 R_{eq}, \tag{3}$$

$$\boldsymbol{i_s} = \boldsymbol{V_s}/\left\{\frac{R_p L_s}{M} + \frac{\omega_0^2 L_s M(R_s + R_{eq})}{(R_s + R_{eq})^2 + \omega_0^2 L_s^2} + j\left[\frac{\omega_0^3 L_s^2 M}{(R_s + R_{eq})^2 + \omega_0^2 L_s^2} - \frac{R_p(R_s + R_{eq}) - \omega_0^2 M^2}{\omega_0 M}\right]\right\}, \tag{4}$$

$$M = k\sqrt{L_p L_s}, \tag{5}$$

where $\boldsymbol{V_s}$ is an RMS value of a fundamental frequency part of an averaged input voltage $v_{in}(t)$, $\boldsymbol{i_s}$ is the secondary circuit side current, and k is a coupling factor between two circuit sides [6]. The resonant frequency ω_0 derivation can be found in [6]. Both $\boldsymbol{i_p}$ and $\boldsymbol{i_s}$ are calculated at resonance of the coupled system given in Fig. 4. The amplitudes (peak values) of V_s and the simplified averaged voltage V_{avg} for the NIM case are

$$V_s = \frac{4V_{avg}}{\pi}, \tag{6}$$

$$V_{avg} = \frac{3V_{amp}}{(2\pi)}, \tag{7}$$

as explained in [4].

3 Successive injection modulation

SIM utilises positive and negative injections successively during 'minimum absolute value' of the three-phase input

$$\text{Min}(v) = \text{Min}(|v_a(t)|, |v_b(t)|, |v_c(t)|)\,. \tag{8}$$

At the condition, two other input phases are at a maximum difference and will be used for such injections. Free-wheeling oscillation is only used when a lower output power is needed.

A modulation illustration is given in Fig. 5, which is also a depiction of a controlled output, due to $v_{in}(t)$ sparseness. The modulation scheme has three different injection voltage levels, which are positive, zero, and negative. Voltage transitions are performed at the zero-crossings of the primary resonant current $i_p(t)$. As in the NIM case, the polarity of injection voltage is always the same as the polarity of the resonant current. The modulation ensures that a positive injection is always accompanied by the negative one in a following order, either directly or through a zero level. When the turn-on is performed very close to a border of a certain Min(v), the turn-off can happen in the other Min(v) region (a turn-off delay effect) to maintain the zero-crossing transitions.

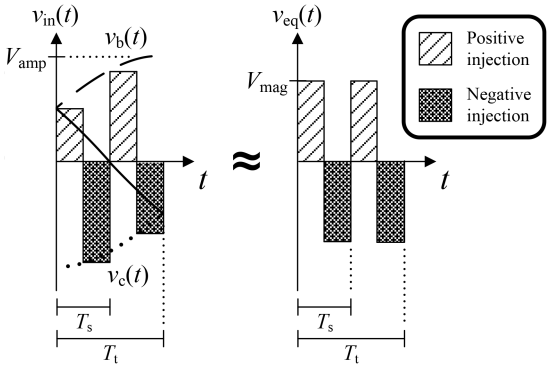

Fig. 6 *Successive injection voltage approximation illustration during Min(v) equals $v_a(t)$. Each phase voltage amplitude is V_{amp}, while V_{mag} is the amplitude of $v_{eq}(t)$*

3.1 Steady-state analysis

Steady-state analysis is used to calculate some variables of SIM using a model given in Fig. 4. The analysis is also based on the same assumptions as in NIM case which are all electric components are ideal, the load is purely resistive, and the converter is at a maximum output capacity configuration. In this case, there are only injections, and the free-wheeling oscillation switch pair Sd (see Fig. 1) is not used.

An equivalent input voltage with a constant amplitude over the primary resonant circuit is needed to simplify all calculations. The idea is to calculate a square voltage $v_{eq}(t)$ that can produce an equal input power as the actual injection voltage $v_{in}(t)$. The equivalent voltage will be approximated through injections illustration during Min(v) equals $v_a(t)$ shown in Fig. 6. Switching period is exaggerated for clarity and marked by T_s, which is the same as the primary resonant current period. Variable T_t indicates the duration of Min(v), which equals to π/3 rad or 3.333 ms for a 50 Hz line frequency. The calculation uses some assumptions which are, $T_s \ll T_t$, $T_t = nT_s$, where $n \in \mathbb{Z}^+$, current $i_p(t)$ has a constant amplitude due to almost uniform injection voltage $v_{in}(t)$, and it also has a zero phase-shift with the $v_{in}(t)$ because of the zero-current switching.

Since the power is a multiplication between voltage and current, the problem becomes geometrical and can be solved through calculating a half area of Min(v)

$$A = \int_{\pi/6}^{3\pi/6} V_{amp}\sin(\varphi)\mathrm{d}\varphi = V_{amp}\sqrt{3}/2. \tag{9}$$

The product of V_{mag} and T_t (π/3 rad) has to equal the area A, therefore,

$$V_{mag}T_t = V_{amp}\sqrt{3}/2, \tag{10}$$

$$V_{mag} = 3V_{amp}\sqrt{3}/(2\pi). \tag{11}$$

Through a Fourier analysis, the fundamental component amplitude of $v_{eq}(t)$ is

$$V_{eq1} = 4V_{mag}/\pi. \tag{12}$$

Output power of NIM can then be calculated using (2)–(4) with $V_s = V_{eq1}$.

The ratio of injection voltage amplitude between NIM and SIM is

$$V_{s(SIM)}/V_{s(NIM)} = V_{mag}/V_{avg} = \sqrt{3}, \tag{13}$$

which equals to 1.732. Subscripts '(NIM)' and '(SIM)' are used to differentiate the variables. The same goes for the RMS ratio of primary and secondary circuit current

Table 1 Converter circuit parameters. Variable *f* is an input line frequency

Parameters	Values
V_{amp}	100 V
f	50 Hz
C_p	0.2 μF
L_p	200 μH
L_s	200 μH
R_p	0.3 Ω
R_s	0.3 Ω
k	0.55
R_L	47.742 Ω
R_{eq}	38.698 Ω

Table 2 Analytical calculation results obtained from MATLAB

	$V_{s\,(RMS)}$	$\lvert i_{p\,(RMS)}\rvert$	$\lvert i_{s\,(RMS)}\rvert$	P_{out}
NIM	42.987 V	7.992 A	2.884 A	321.893 W
SIM	74.456 V	13.843 A	4.995 A	965.679 W

$$i_{z(SIM)}/i_{z(NIM)} = V_{mag}/V_{avg} = \sqrt{3}, \tag{14}$$

where subscript 'z' indicates either it belongs to the primary or the secondary side. The ratio between SIM and NIM average output power with the same circuit parameters can be calculated as follows

$$P_{out(SIM)}/P_{out(NIM)} = V^2_{s(SIM)}/V^2_{s(NIM)} = 3. \tag{15}$$

Therefore, with the previous assumptions for steady-state analysis, the output power amplification of a SIM case compared to the NIM case is three times.

3.2 Analytical calculations

The analytical output power for both modulations are further calculated using a MATLAB software based on circuit schematic given in Fig. 4. Circuit parameters are provided in Table 1, and they are obtained from a component selection explained in [5, 6].

The results of analytical calculation are presented in Table 2. The voltage and current values are in RMS form, while the output powers are an average value.

4 Simulation results

Simulation model was made in PLECS software to validate the theoretical calculations. It will also be used to compare NIM and SIM cases as well as analyse converter influence to the grid side.

4.1 Maximum output capacity comparison

Both NIM and SIM switching actions as well as their steady-state variables will be compared. The circuit parameters used in the simulation model are based on Table 1. The results to show the switching actions of the converter are provided in Figs. 7 and 8. In the NIM case, the steady-state RMS value for the primary and secondary resonant currents are 8.075 and 2.907 A correspondingly. For the SIM case, the values are 13.923 and 5.01 A. In both cases, the primary current is always bigger than the secondary one. The values are also similar to analytical results given in Table 2. The ratio of currents between both modulations is around 1.72 which is very close to the one in (14). In terms of switching, the injection of NIM is mostly accompanied by a free-wheeling oscillation. In SIM, the positive and negative injections are performed all the time, thus the Sd switch pair (see Fig. 1) is not utilised in this case. It can be observed that the switching transition happens at the zero-crossing of the resonant current. The resonant frequency for both cases is around 26.81 kHz.

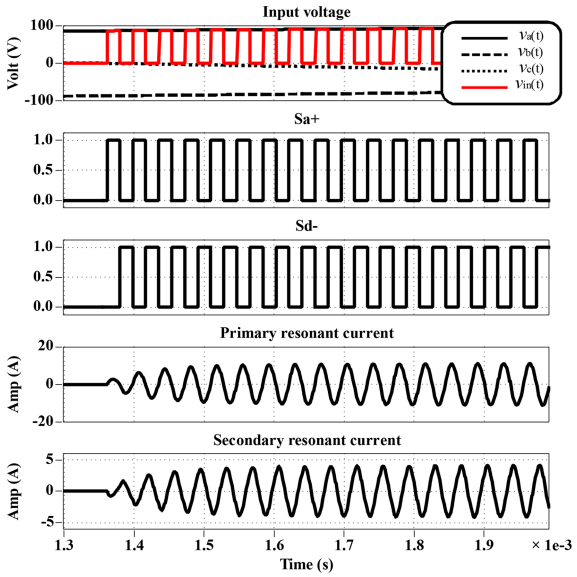

Fig. 7 *Switching actions of NIM during Max(v) equals $v_a(t)$. Injection from Sa + is always accompanied by a free-wheeling oscillation of Sd-*

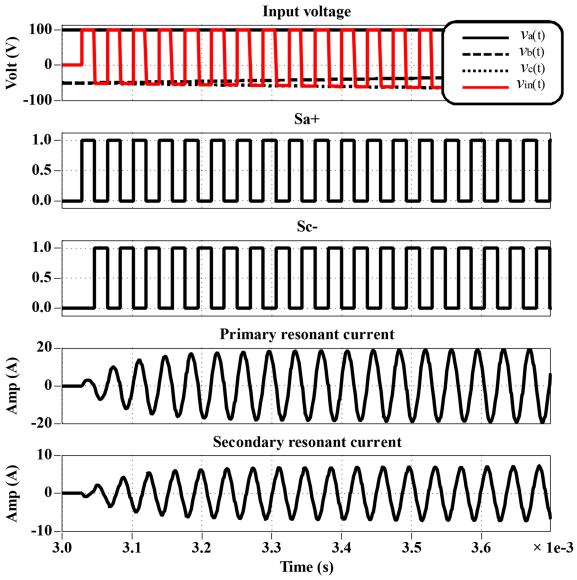

Fig. 8 *Switching actions of SIM during Min(v) equals $v_b(t)$. Positive injection from Sa + is always accompanied by the negative one from Sc-*

Average output power plots of two modulation strategies are shown in Fig. 9. The steady-state average value for NIM is 327.118 W and for SIM is 971.211 W. The values are also similar to analytical results in Table 2. The SIM output power capacity is 2.969 times the NIM case, which is very close to 3 as was predicted in the steady-state analysis section.

4.2 Input and ground currents observation

Under a SIM operation, input and ground currents for open-loop and closed-loop cases are also observed to anticipate their influence to power grid. The open-loop case uses maximum output capacity configuration. In the closed-loop case, an on-off current controller is used in the simulation to control the primary resonant current amplitude. The controller uses a free-wheeling oscillations to reduce the amplitude.

For the open-loop case, the waveforms are plotted in Fig. 10. It can be seen that the converter needs an input filter to limit distortion effects to a connected power grid. The steady-state ground current mean value in this case is 3.125 mA. It should be taken into account that the switching frequency is synchronised with the resonant frequency, and it is influenced by the coil distance.

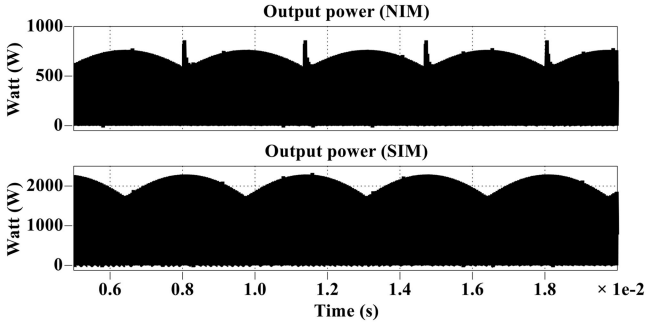

Fig. 9 *Output power waveforms of NIM and SIM*

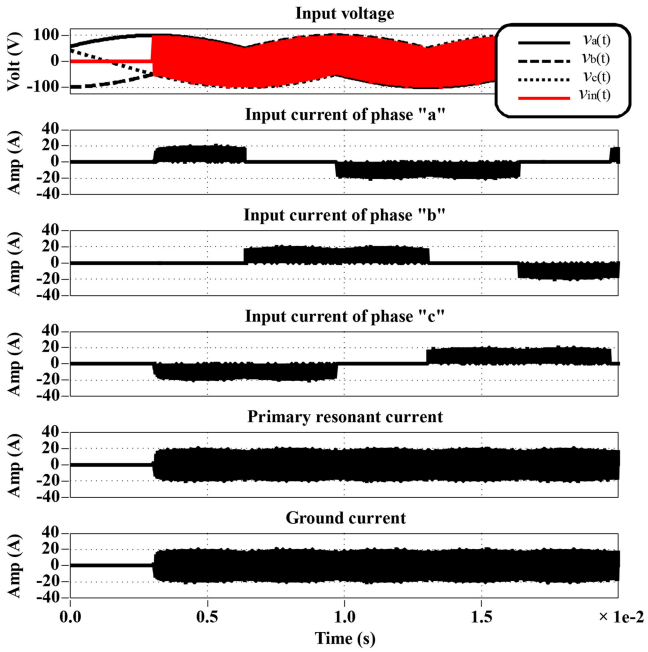

Fig. 10 *Input and ground currents plots of SIM case under an open-loop condition*

When an on-off current controller is used in the converter with a set-point (reference) value of 5 A, the converter produces some waveforms given in Fig. 11. The current waveforms become sparse due to a less frequent injections applied by the converter. The RMS value of the primary resonant current is 6.083 A, while the steady-state ground current mean value is 29.322 mA. This indicates that there is a relationship between a controlled modulation and the ground current waveform. Further investigation of the relationship will be done in future publications.

5 Conclusions

A SIM method for a direct three-phase to single-phase AC/AC converter has been presented here. The modulation has three voltage levels which are positive, zero, and negative. Compared to an NIM, the proposed modulation produces 1.72 times primary and secondary resonant currents and three times output power with the same circuit setup. Simulation results confirm the validity of analytical calculations. The results also show that a good electromagnetic interference (EMI) filter is needed in a practical application. However, an on-off current controller might not be suitable for the modulation since it increases a DC current on the ground line at a certain set-point. Experimental equipment are currently being built. Measurement data and analysis will be reported in future publications.

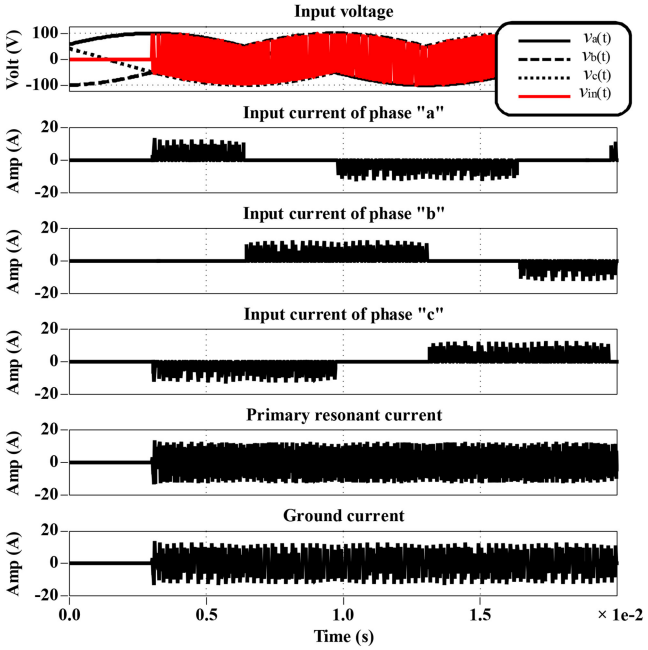

Fig. 11 *Input and ground currents plots of SIM case produced by an on-off current controller with a set-point of 5 A*

6 References

[1] Bac, N.X., Vilathgamuwa, D.M., Madawala, U.K., *et al.*: 'A matrix converter based inductive power transfer system'. Proc. Int. Power and Energy Conf., Ho Chi Minh City, Vietnam, December 2012, pp. 509–514

[2] Bac, N.X., Vilathgamuwa, D.M., Madawala, U.K., *et al.*: 'A SiC-based matrix converter topology for inductive power transfer system', *IEEE Trans. Power Electron.*, 2013, **29**, (8), pp. 4029–4038

[3] Huang, C., James, J.E., Covic, G.A., *et al.*: 'Design considerations for variable coupling lumped coil systems', *IEEE Trans. Power Electron.*, 2015, **30**, (2), pp. 680–689

[4] Kusumah, F.P., Vuorsalo, S., Kyyrä, J., *et al.*: 'A direct three-phase to single-phase AC/AC converter for contactless electric vehicle charger'. Proc. European Conf. on Power Electronics and Applications, Geneva, 2015, pp. 1–10

[5] Kusumah, F.P., Vuorsalo, S., Kyyrä, J., *et al.*: 'Components selection of a direct three-phase to single-phase AC/AC converter for a contactless electric vehicle charger'. Proc. European Conf. on Power Electronics and Applications, Karlsruhe, 2016, pp. 1–10

[6] Kusumah, F.P., Kyyrä, J.: 'Minimizing coil power loss in a direct three-phase to single-phase AC/AC converter-based contactless electric vehicle charger'. Proc. European Conf. on Power Electronics and Applications, Warsaw, 2017, pp. 1–10

[7] Hu, A.P., Li, H.L.: 'A new high frequency current generation method for inductive power transfer applications'. Proc. IEEE Power Electronics Specialists Conf., Jeju, South Korea, June 2006, pp. 1–6

[8] Li, H.L., Hu, A.P., Covic, G.A, *et al.*: 'FPGA controlled high frequency resonant converter for contactless power transfer'. Proc. IEEE Power Electronics Specialists Conf., Rhodes, Greece, 2008, pp. 3642–3647

[9] Li, H.L., Hu, A.P., Covic, G.A, *et al.*: 'A direct AC–AC converter for inductive power-transfer systems', *IEEE Trans. Power Electron.*, 2011, **27**, (2), pp. 661–668

[10] Steigerwald, R.L.: 'A comparison of half-bridge resonant converter topologies', *IEEE Trans. Power Electron.*, 1988, **3**, (2), pp. 174–182